Supporting Information

A 3D luminescent Zn(II) MOF for the detection of high explosives and the degradation of organic dyes: an experimental and computational study

Jun-Cheng Jin[a], Jian Wu[b], Jing-Xin Zhang[c], Bao-Hong Li[c]*, Jian-Qiang Liu[c], Rajendra Prasad,[d] Abhinav Kumar[e*] and Stuart R. Batten[f]

Photoluminescence measurements

The photoluminescence sensing experiments were performed as follows: the photoluminescence properties of **1** were investigated in DMF/H_2O emulsions at room temperature using a RF-5301PC spectrofluorophotometer. The suspensions were prepared by adding 3 mg of **1**powders into 3 mL of DMF/H_2O and then ultrasonic agitation the mixture for 30 min before testing.

Photocatalytic Method

The photocatalytic reactions were performed as follows: 50mg of **1** were dispersed in 50 mL aqueous solution of RhB/MV (10 mg/L) under stirring in the dark for 30 min to ensure the establishment of an adsorption-desorption equilibrium. Then the mixed solution was exposed to UV irradiation from an Hg lamp (250 W) and kept under continuous stirring during irradiation for 100 min. Samples of 5mL were taken out every 10 min and collected by centrifugation for analysis by UV-Vis spectrometer. By contrast, the simple control experiment was also performed under the same condition without adding any catalysts.

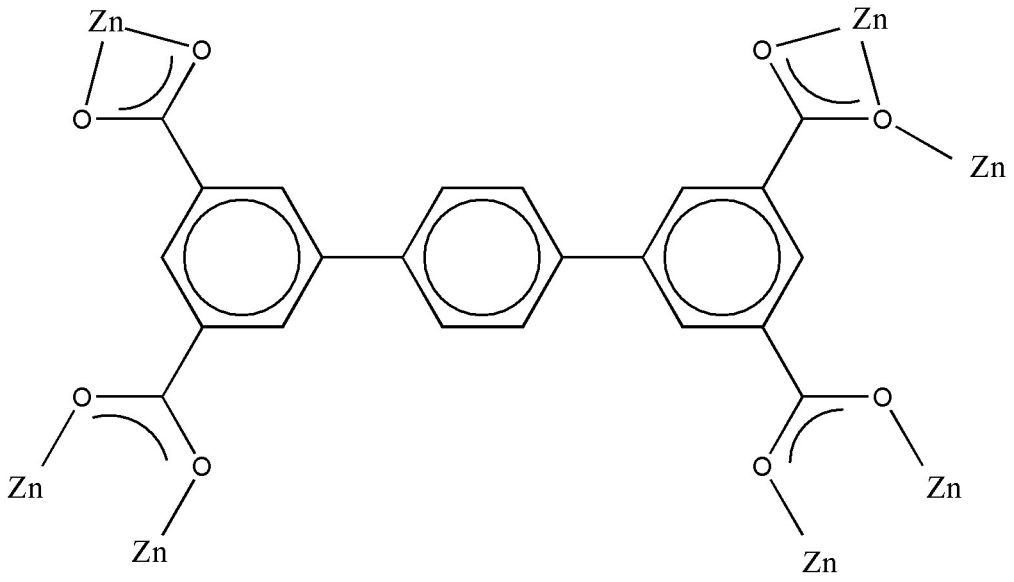

Scheme S1 View of the possible coordination modes of L^{4-} ligand used in this work.

Thermal Analysis

The thermal stabilities of crystalline samples of **1** were measured under a nitrogen atmosphere (Fig. S1). For **1**, a weight loss of 31.2 % was observed from the room temperature to 400 °C, which corresponds to the loss of coordinated water molecules, coordinated DMF and free DMF molecules (calcd. 33.8 %). Later, the decomposition of framework occurs. The final residuum is ZnO.

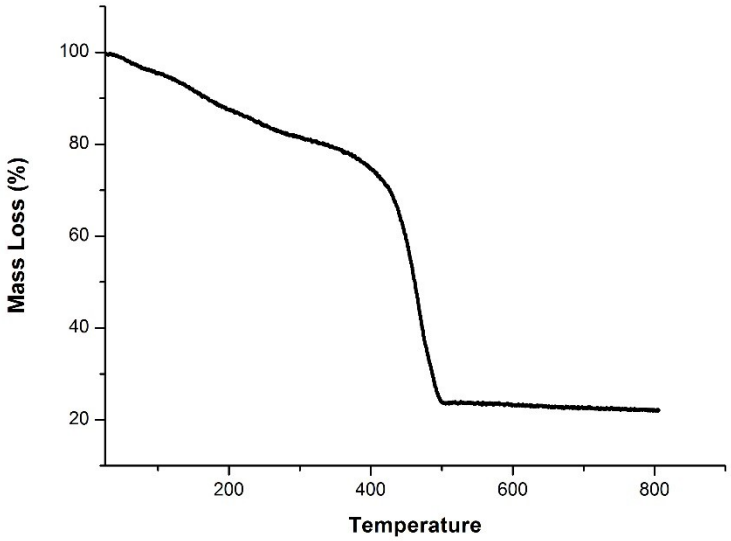

Fig. S1 The TGA plot for **1**.

Measurements

The activated samples were prepared by soaking the as-synthesized samples in CH_3OH for two days, then in CH_2Cl_2 for three days and subsequent heating at 100 ºC in a quartz tube under high vacuum for 20 h to remove the solvent molecules prior to measurements. The nitrogen adsorption-desorption measurements were carried out at liquid nitrogen temperature (77 K) by using automatic volumetric adsorption equipment (Micromeritics, ASAP2020).

The N_2 sorption for **1** has been measured at 77 K and exhibits type I isotherm (Fig. S2), indicating that **1** is a microporous material with pore volume of 334.94 cm^3 (STP) g^{-1} and the BET surface area is 1046.01 m^2/g.

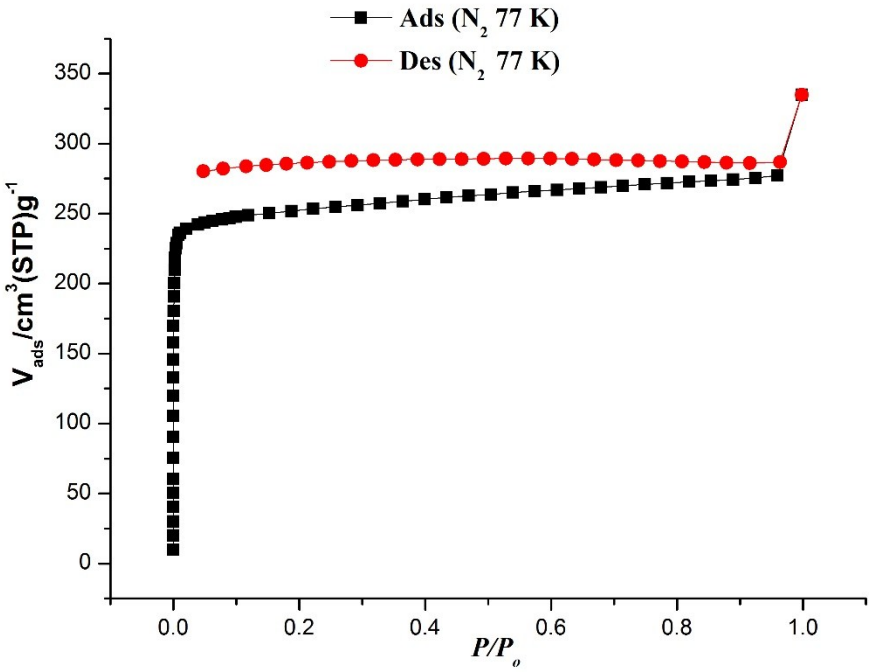

Fig. S2 The N_2 adsorption isotherms at 77 K for **1.**

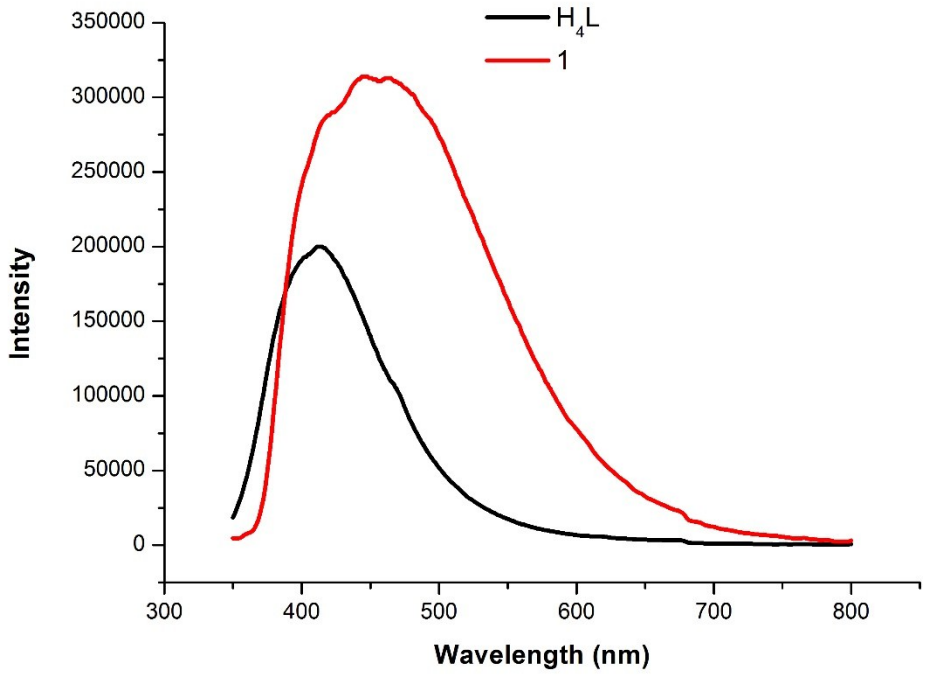

Fig. S3 The photoluminescence spectra of solid samples of H_4L ligand and **1** recorded at room temperature (λ_{ex} =290 nm).

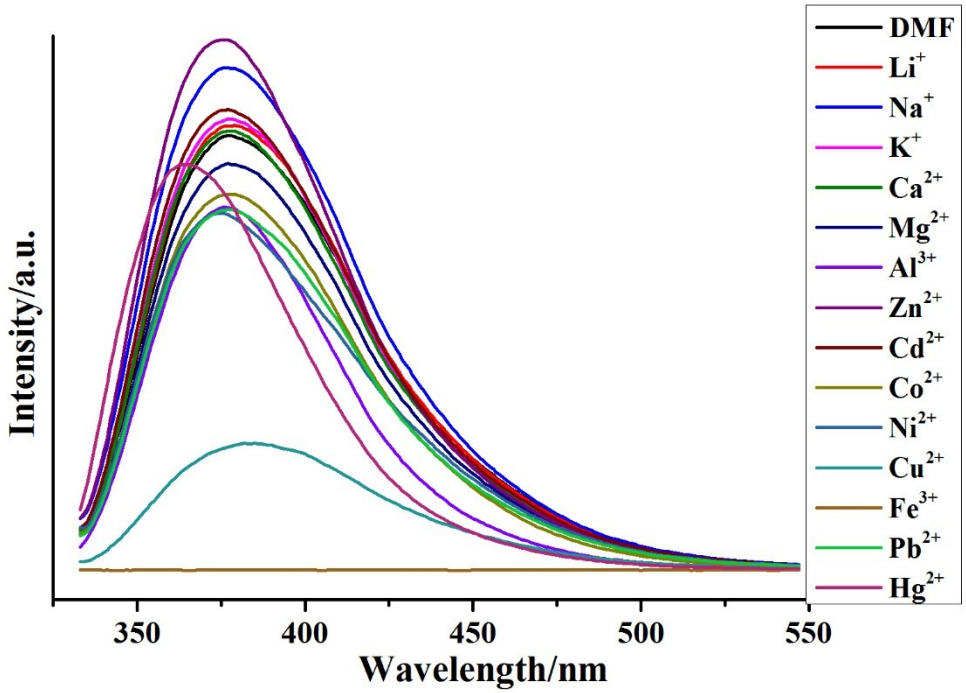

Fig. S4 The photoluminescence intensities spectra of **1** that was dispersed in the solutions of different metal ion

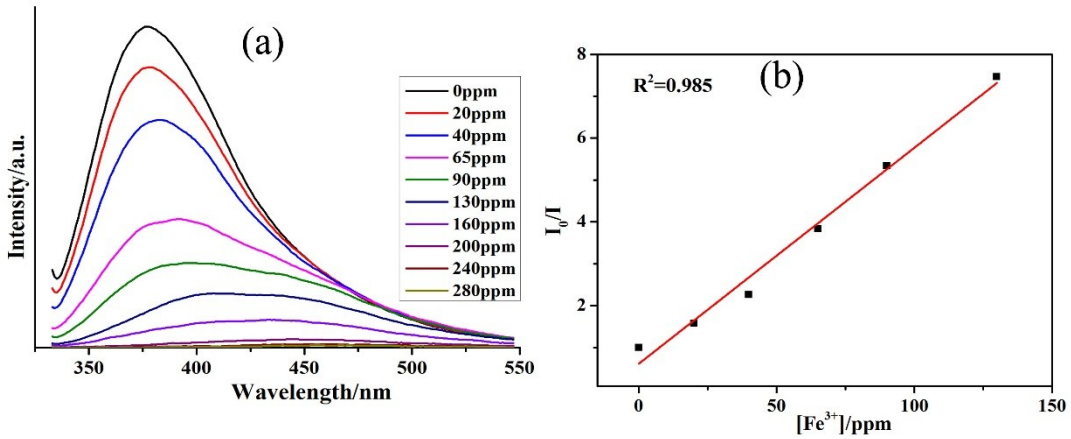

Fig. S5 (a) The emissive responses of **1** against Fe^{3+} in DMF solution with different concentrations; (b) Plot of intensity versus Fe^{3+} concentration.

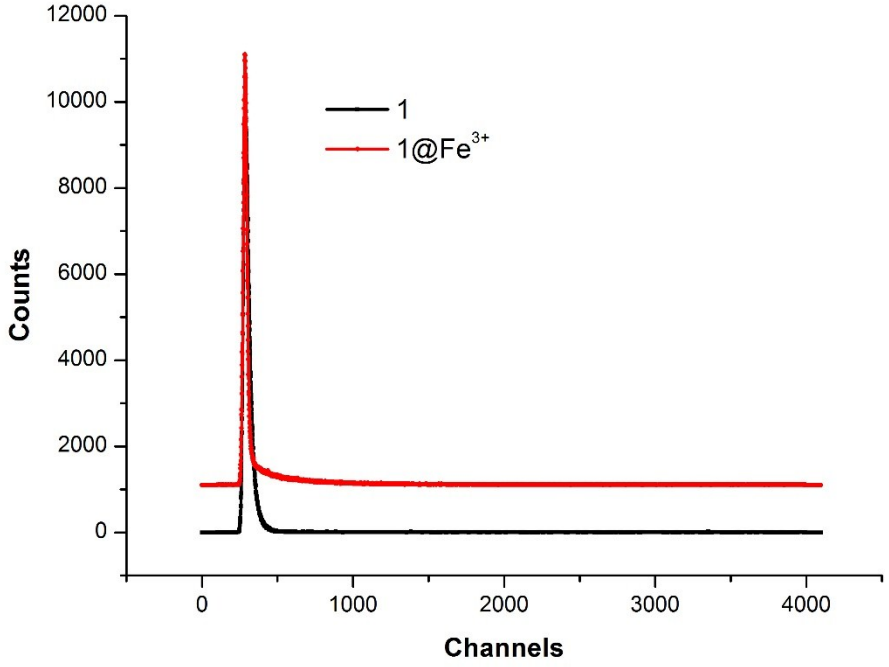

Fig. S6 Comparison of the fluorescence lifetimes of the original sample (black) and Fe^{3+}@ **1** suspension (red).

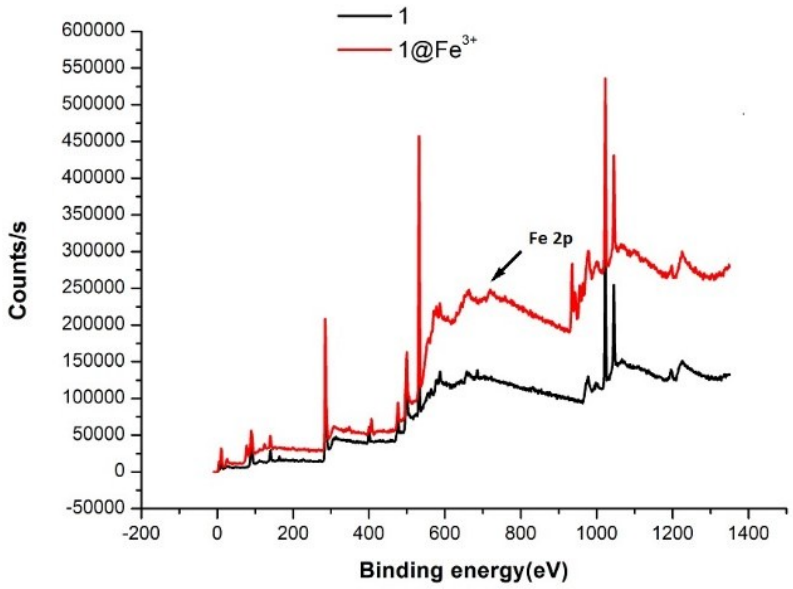

Fig. S7 The XPS spectra of the **1**@Fe^{3+} (red) and **1** (black).

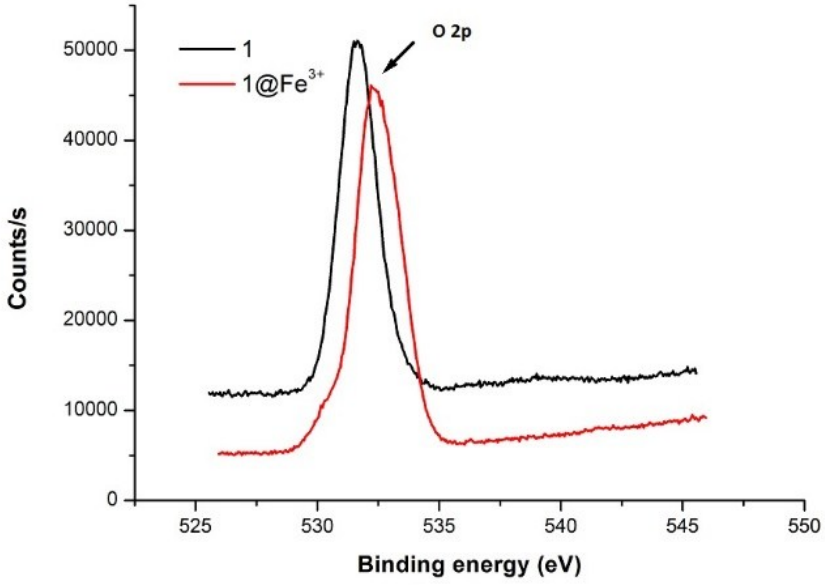

Fig. S8 The O1s XPS spectra of the **1** (black) and **1**@Fe^{3+} (red).

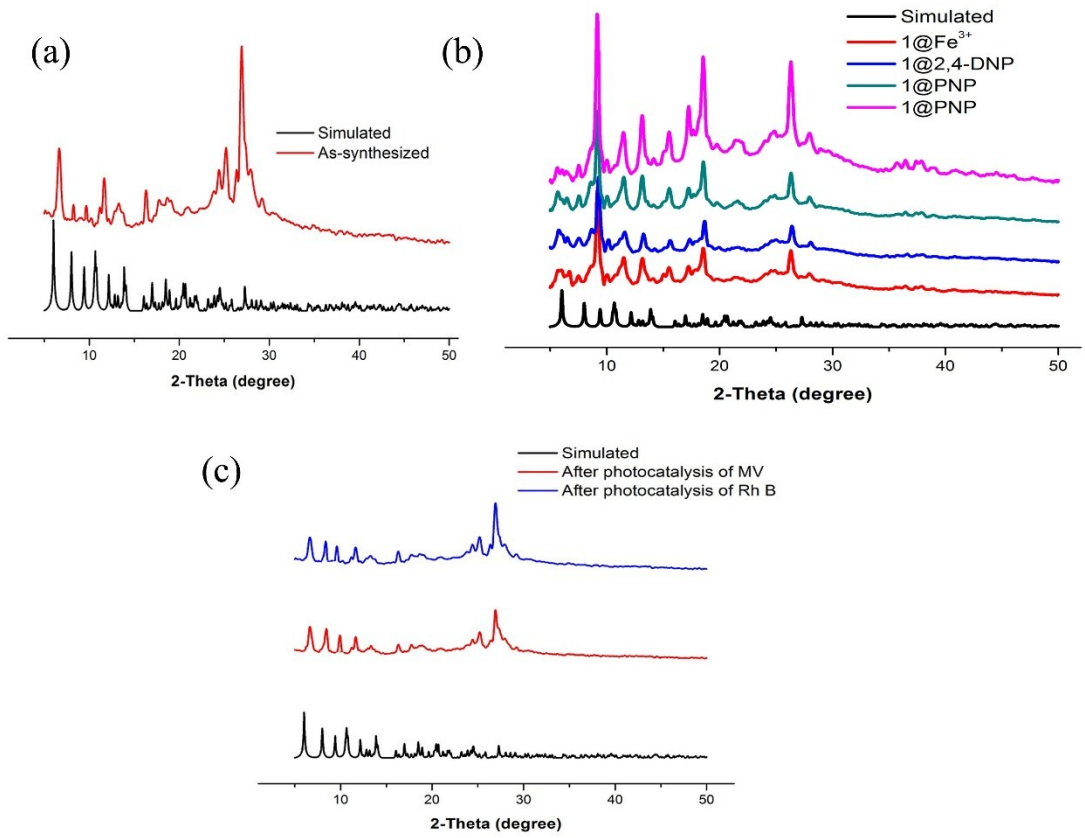

Fig. S9 (a) Powder X-ray diffraction (PXRD) plots of **1** simulated (black) and as-synthesized (red). (b) PXRD patterns of **1** simulated (black) and representative metal ion/explosives-infused **1**. (c) PXRD of **1** (black) and dye-infused **1**.

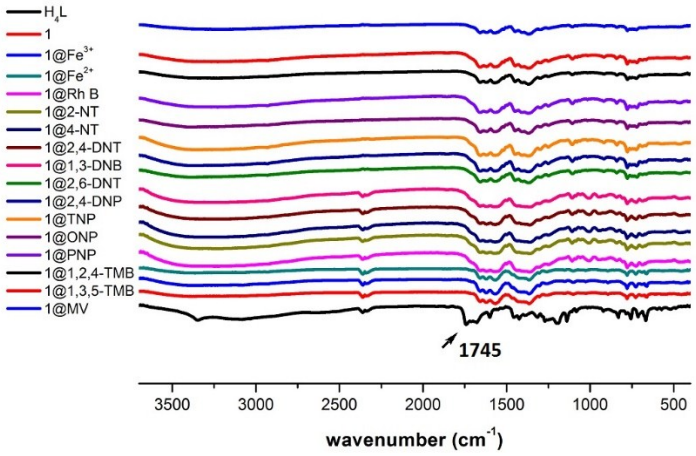

Fig. S10 The IR spectra of **1**, H_4L as well as **1**@Fe^{3+}, **1**@Fe^{2+} as well as **1**@ACs (ACs = nitro-aromatic and aromatic compounds).

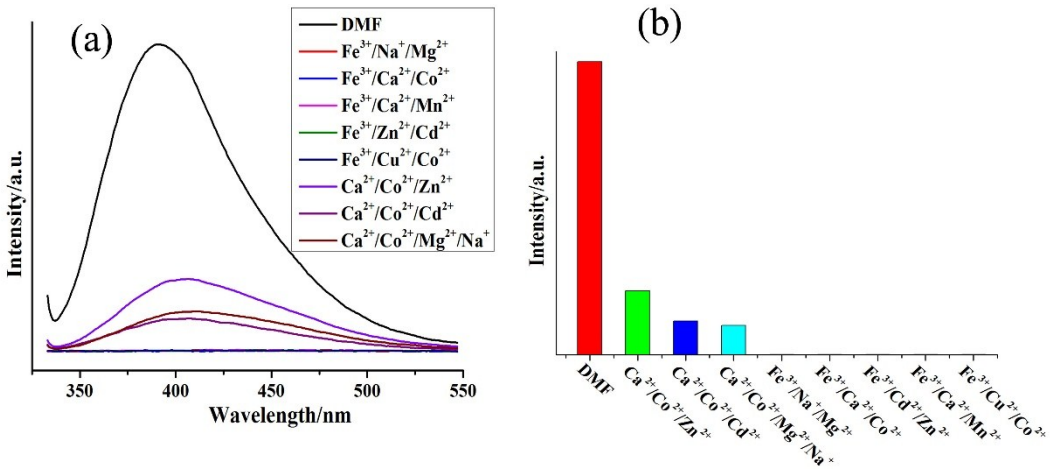

Fig. S11 (a) The photoluminescence intensities spectra of **1** that as dispersed in different metal ion solutions; (b) The view of bar graph for the photoluminescence intensities responses of **1** under mixture metal ion solutions

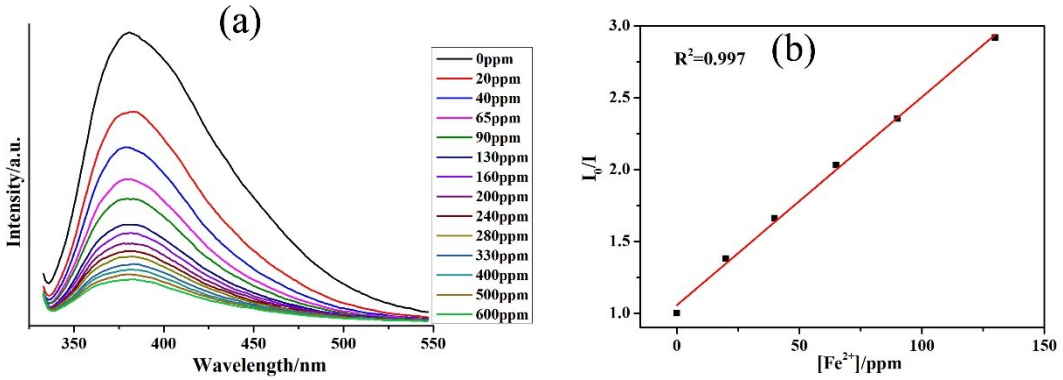

Fig. S12 (a) The emissive response spectra of **1** for Fe^{2+} in DMF solution with different concentrations; (b) Plot of intensity versus Fe^{2+} concentration.

.

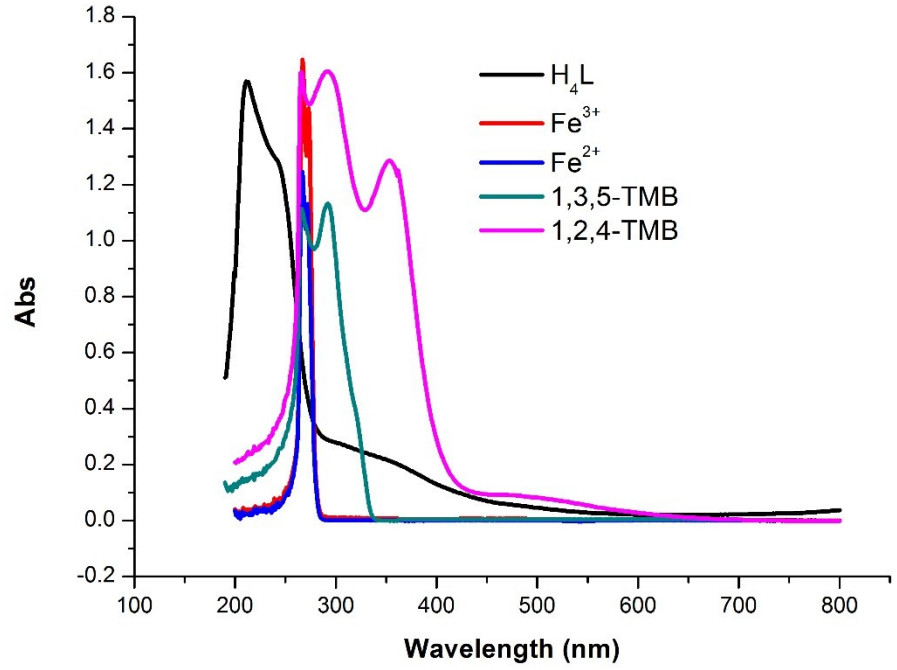

Fig. S13 The UV-Vis spectra for different analytes and ligand.

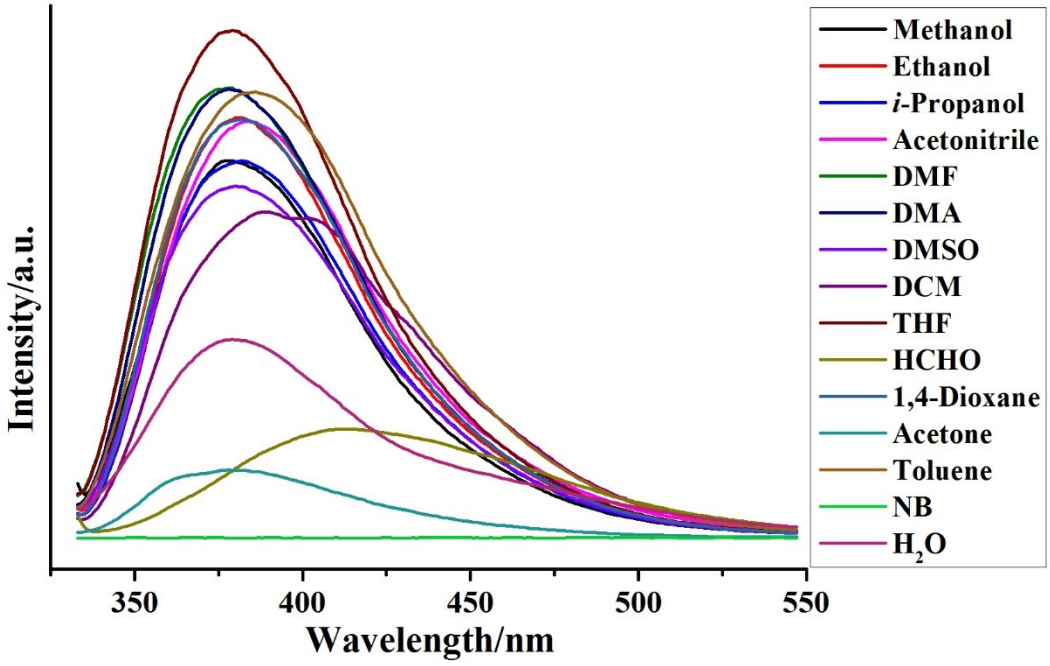

Fig. S14 The photoluminescence intensity spectra of **1** that were dispersed in different organic solvents.

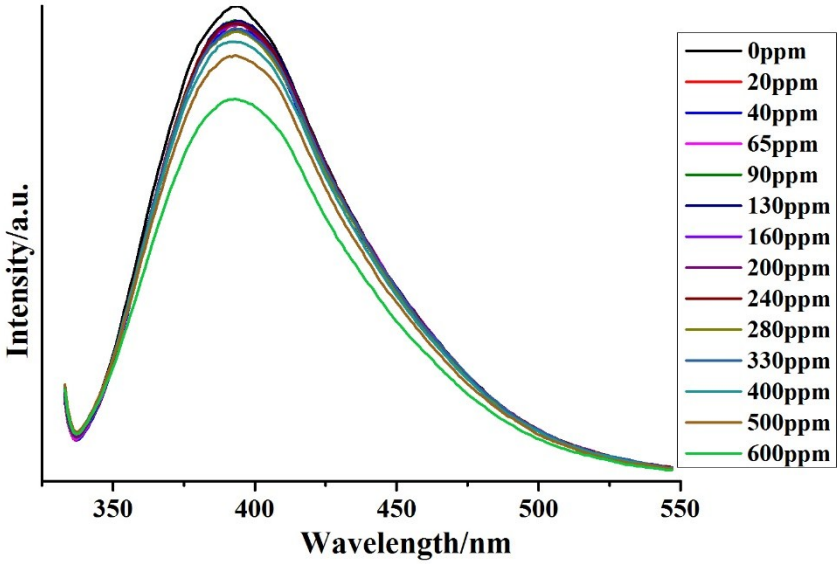

Fig. S15 The emissive responses of **1** for 1,2,4-TMB in DMF solution with different concentrations.

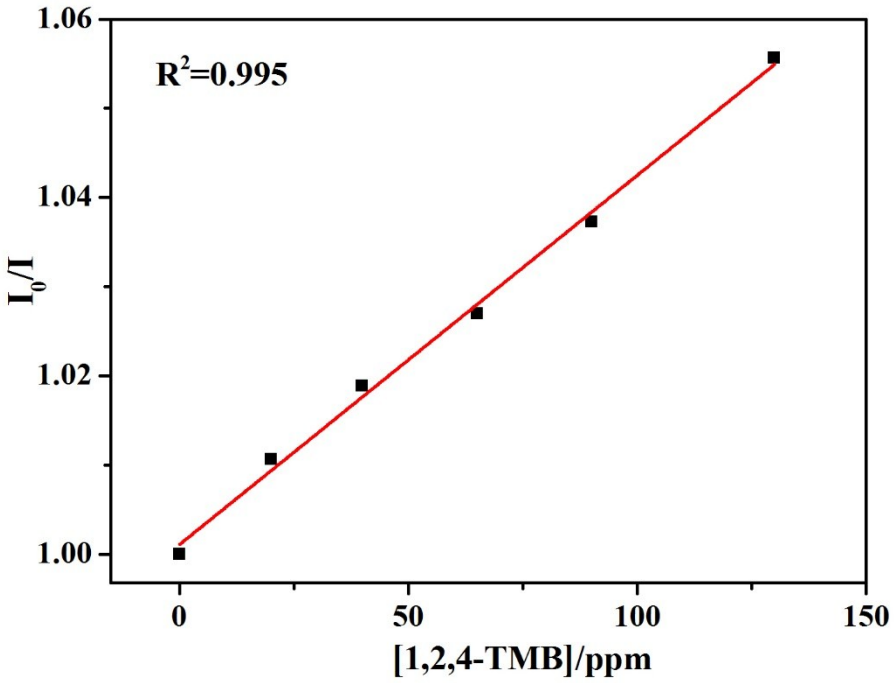

Fig. S16 The Stern–Volmer plot of **1** against 1,2,4-TMB.

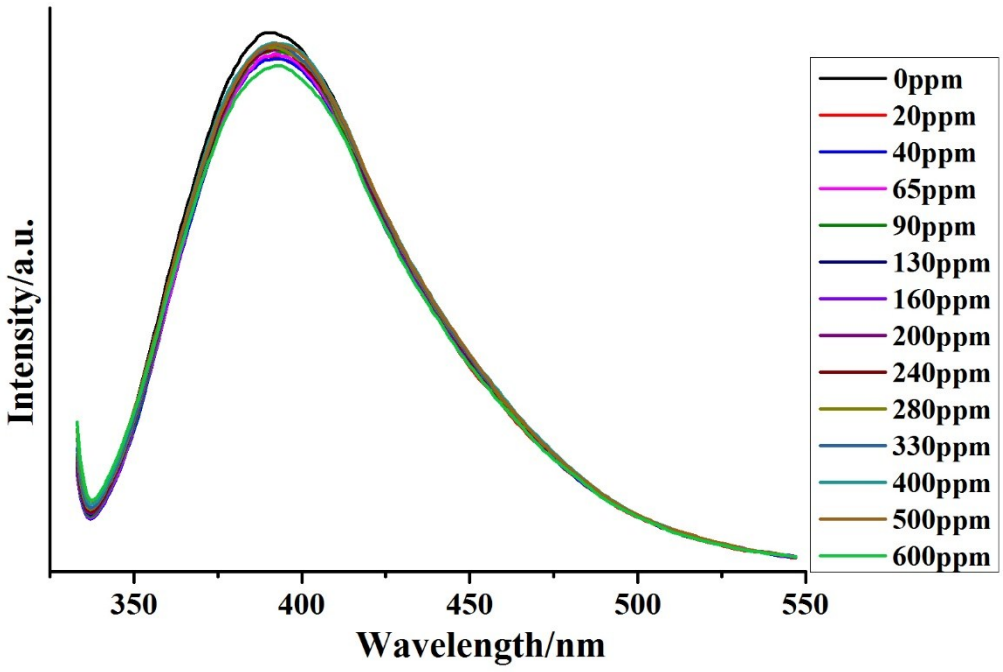

Fig. S17 The emissive responses of **1** for 1,3,5-TMB in DMF solution with different concentrations.

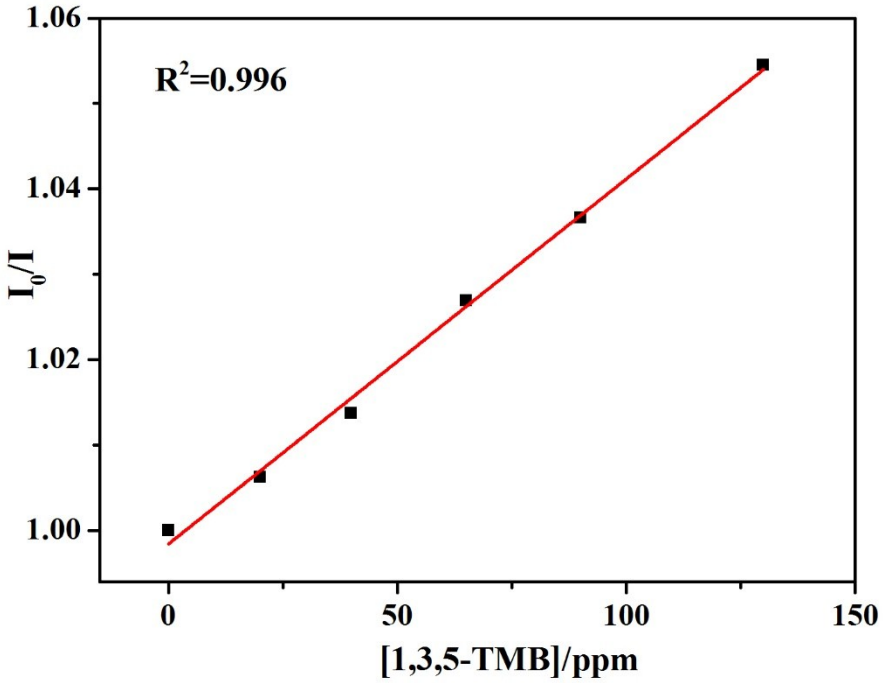

Fig. S18 The Stern–Volmer plot of **1** against 1,3,5-TMB.

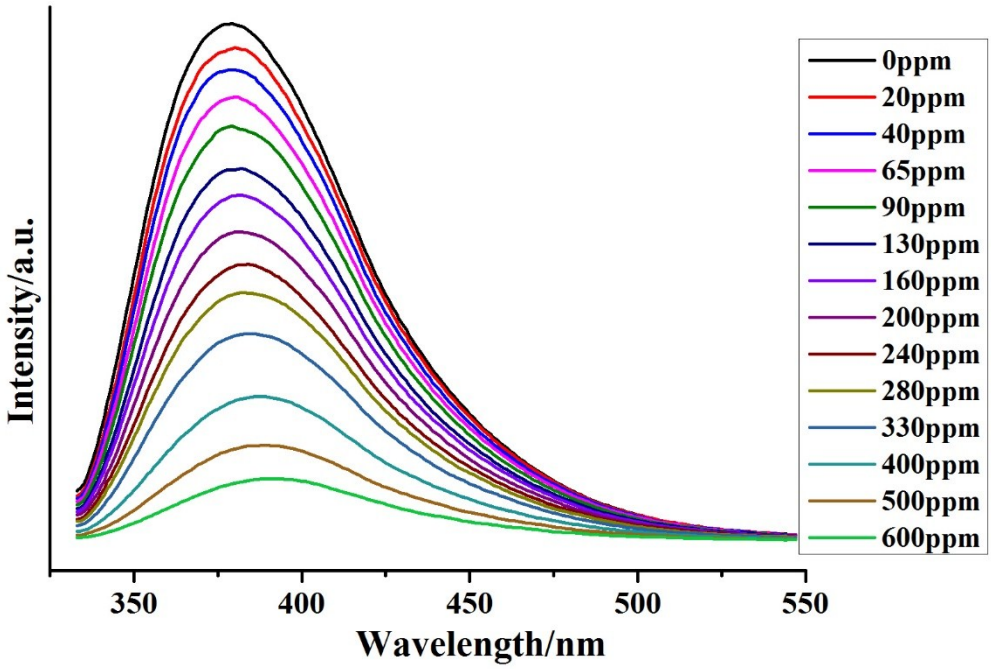

Fig. S19 The emissive responses of **1** for 1,3-DNB in DMF solution with different concentrations.

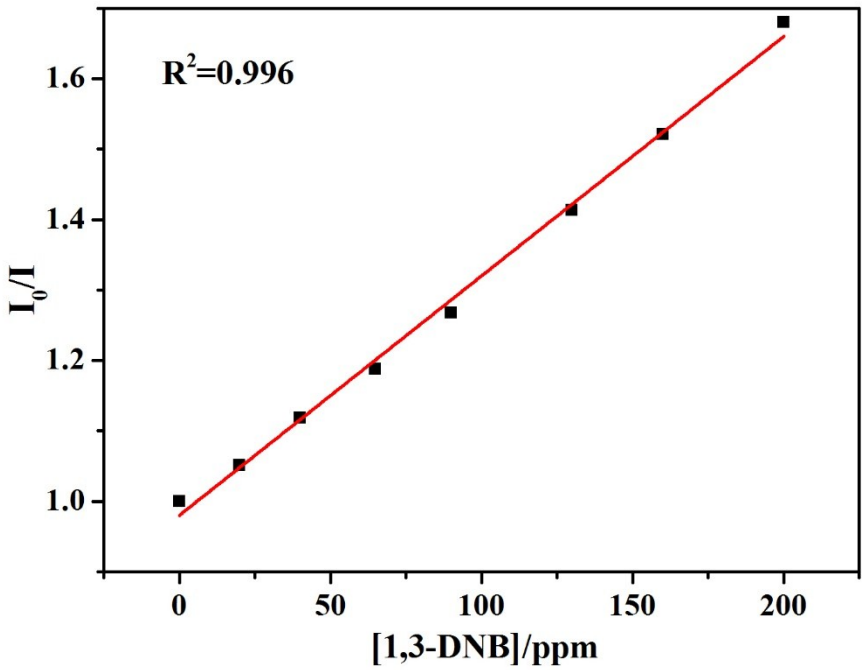

Fig. S20 The Stern–Volmer plot of **1** against 1,3-DNB.

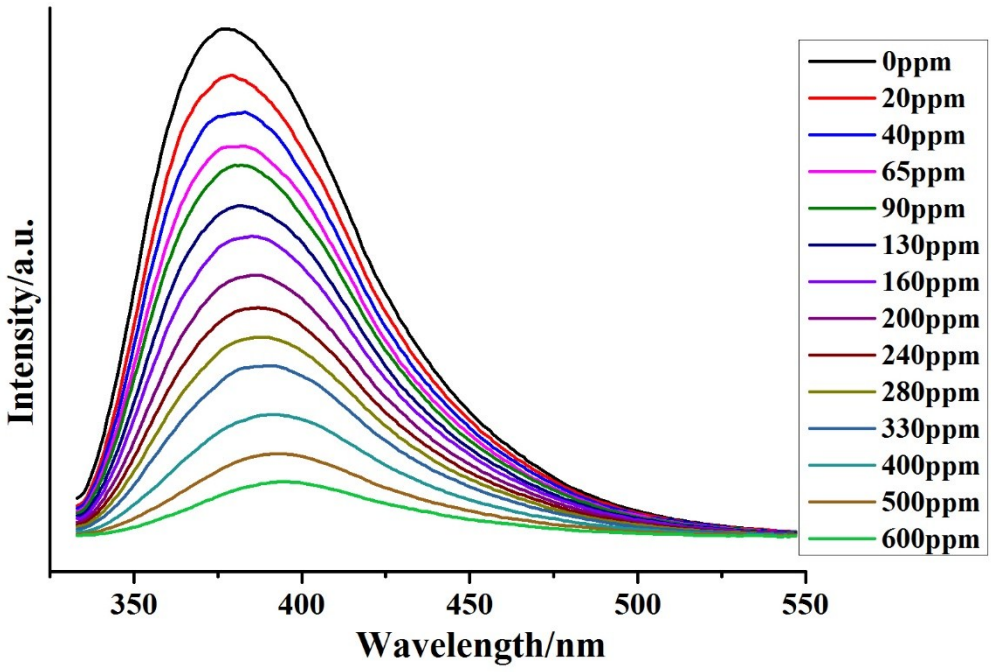

Fig. S21 The emissive responses of **1** for 2,4-DNT in DMF solution with different concentrations.

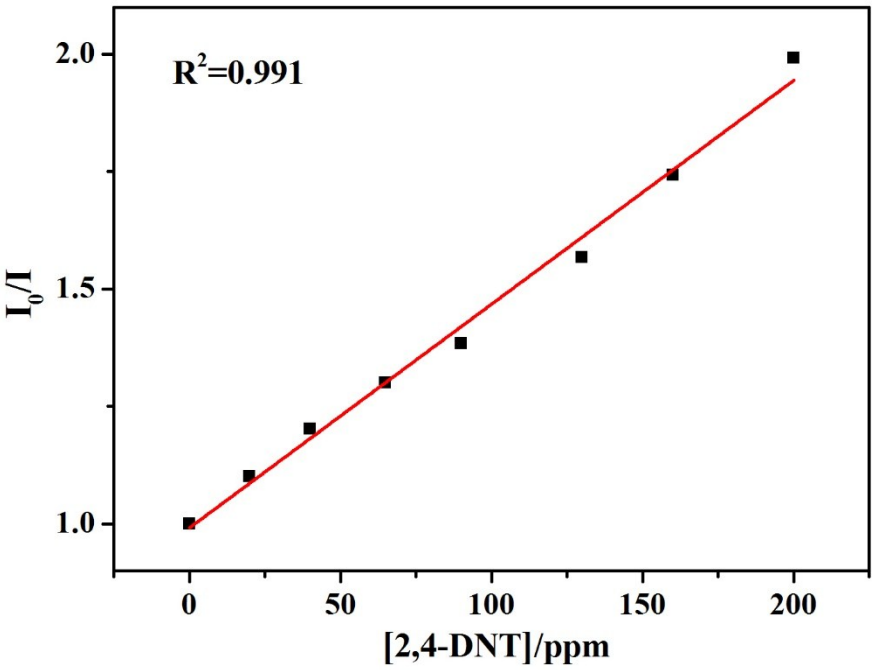

Fig. S22 The Stern–Volmer plot of **1** against 2,4-DNT.

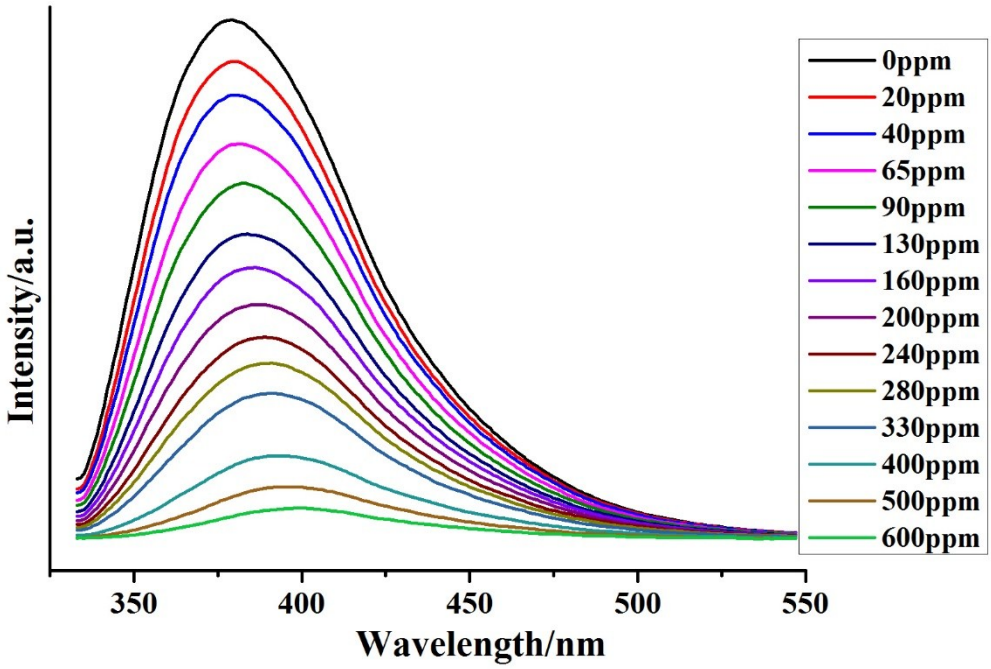

Fig. S23 The emissive responses of **1** for 2,6-DNT in DMF solution with different concentrations.

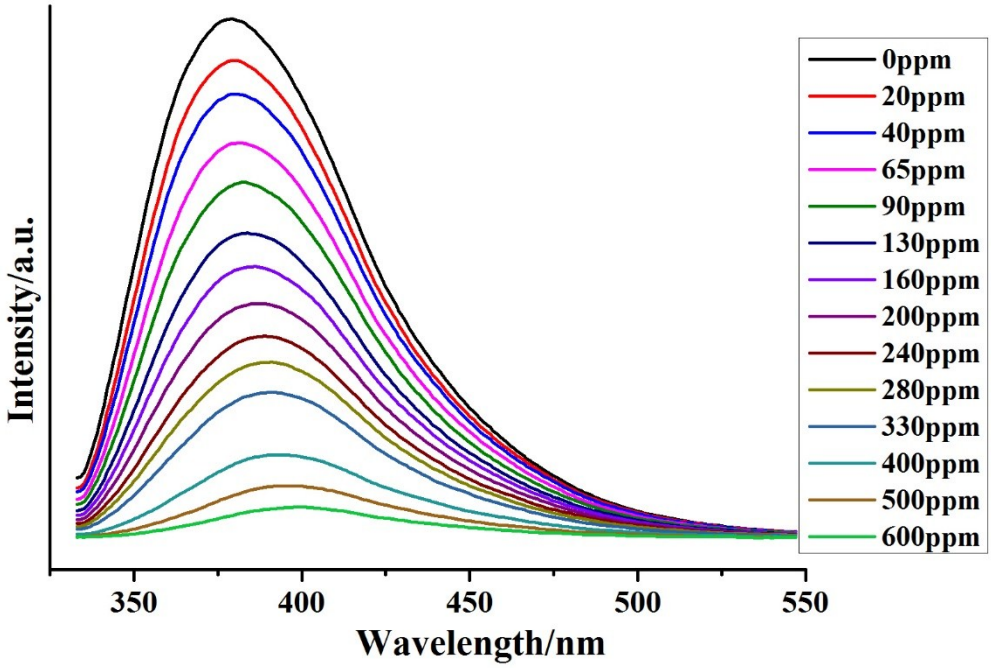

Fig. S24 The Stern–Volmer plot of **1** against 2,6-DNT.

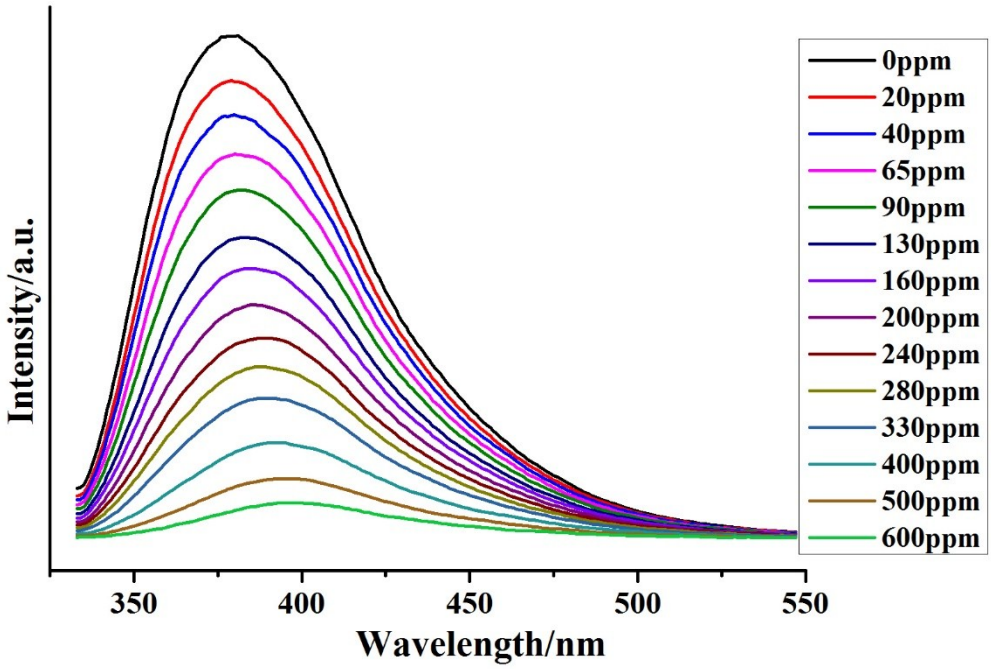

Fig. S25 The emissive responses of **1** for 2-NT in DMF solution with different concentrations.

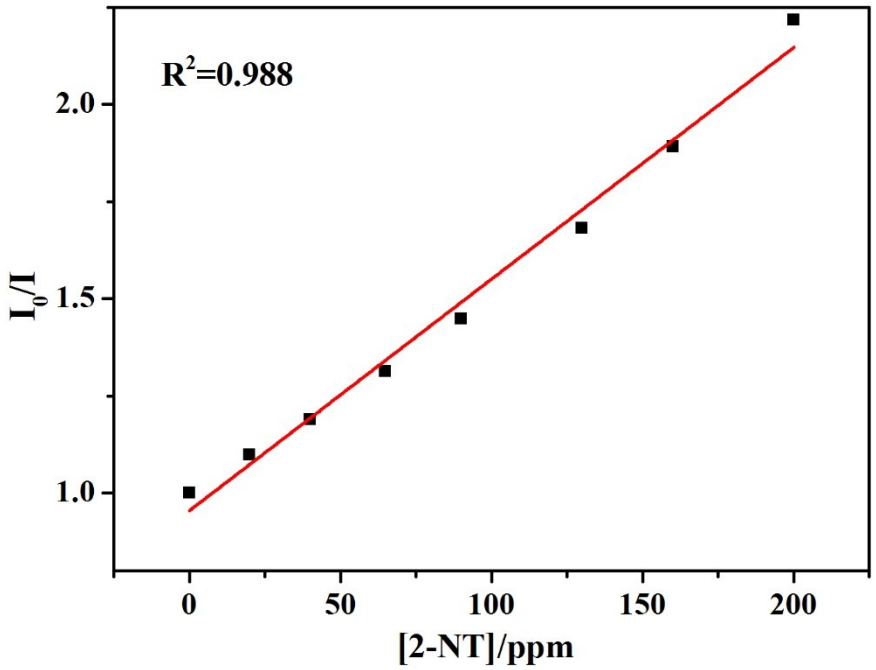

Fig. S26 The Stern–Volmer plot of **1** against 2-NT.

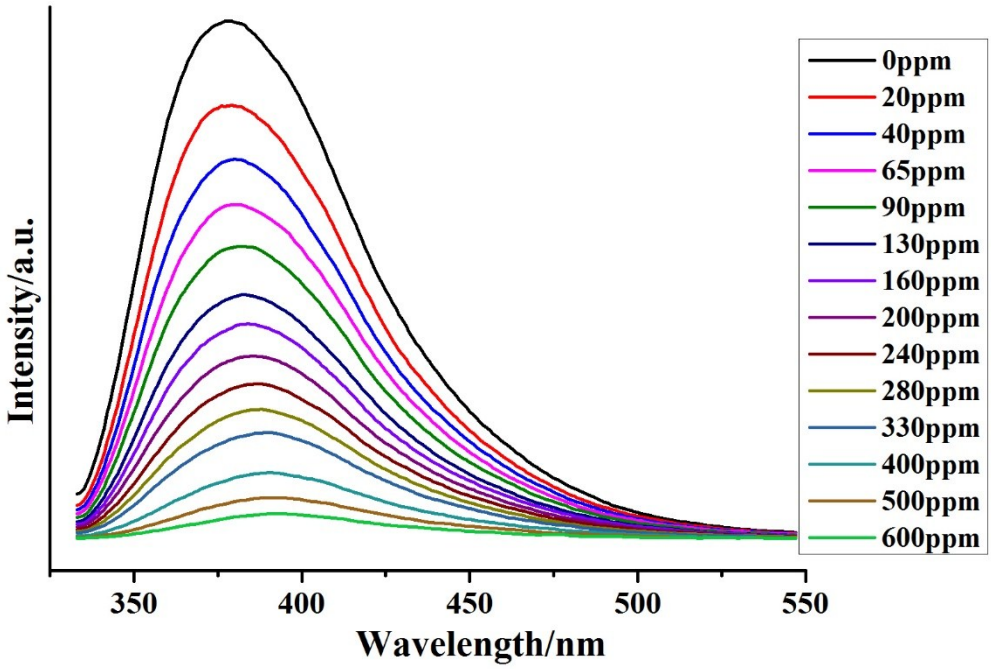

Fig. S27 The emissive responses of **1** for 4-NT in DMF solution with different concentrations.

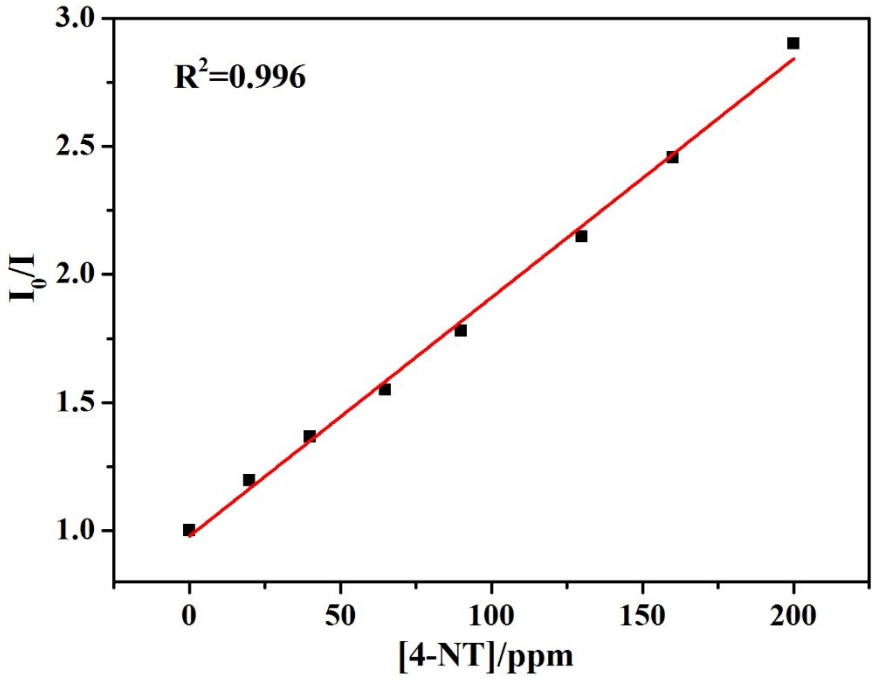

Fig. S28 The Stern–Volmer plot of 1 against 4-NT.

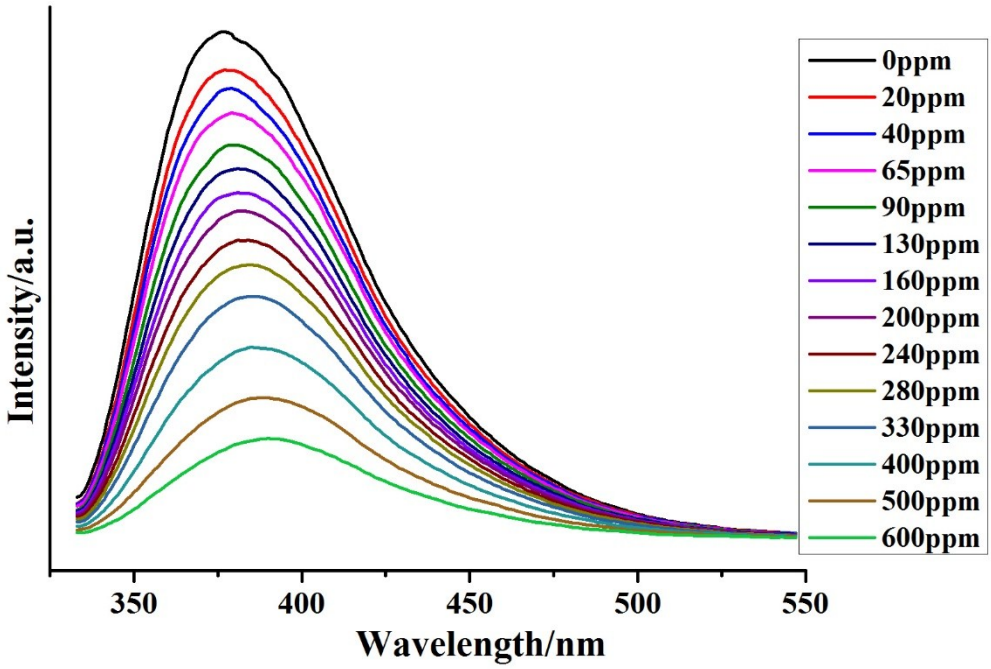

Fig. S29 The emissive responses of **1** for NB in DMF solution with different concentrations.

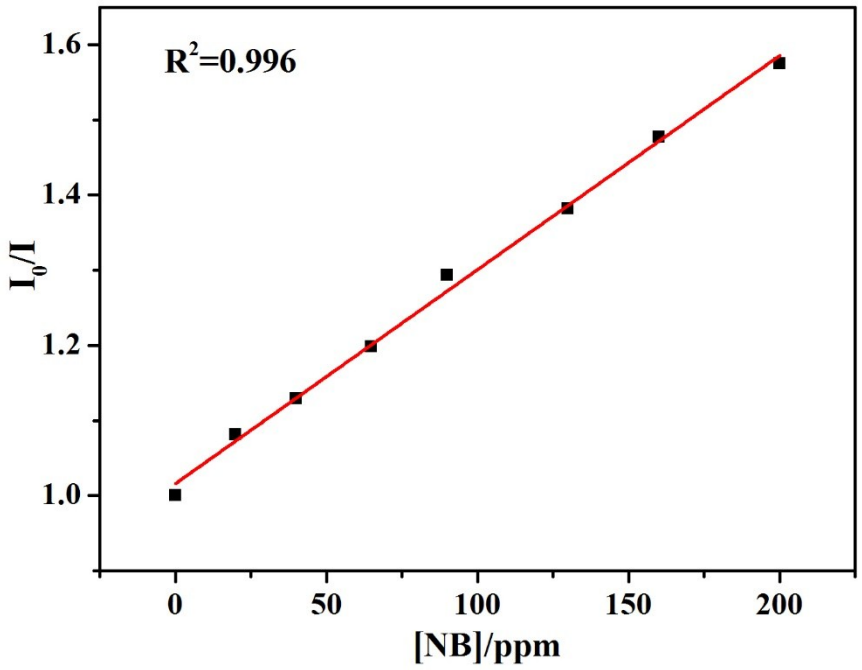

Fig. S30 The Stern–Volmer plot of **1** against NB.

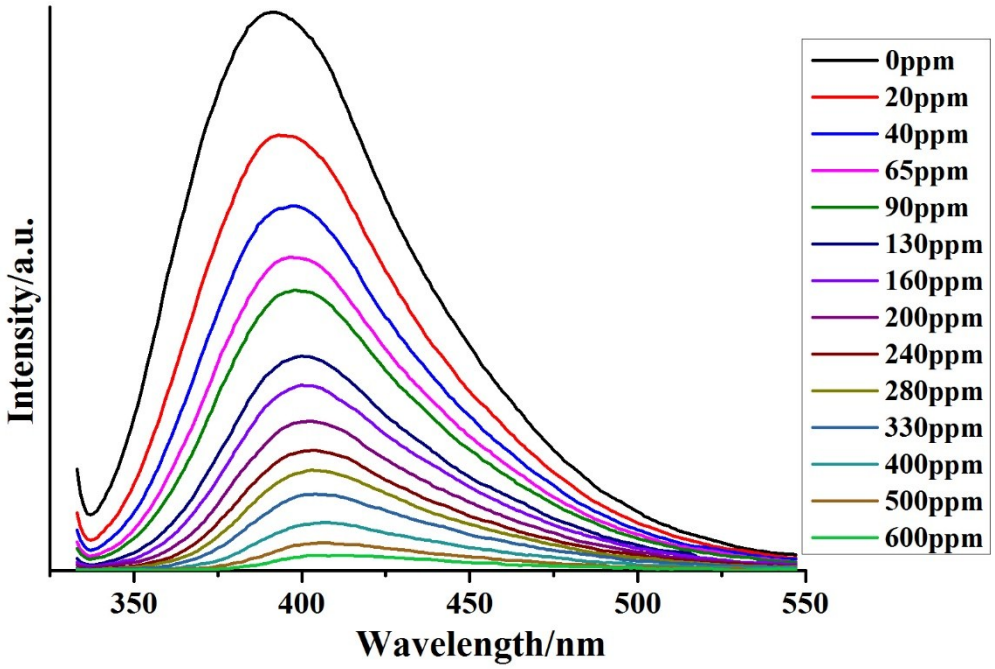

Fig. S31 The emissive responses of **1** for MNP in DMF solution with different concentrations.

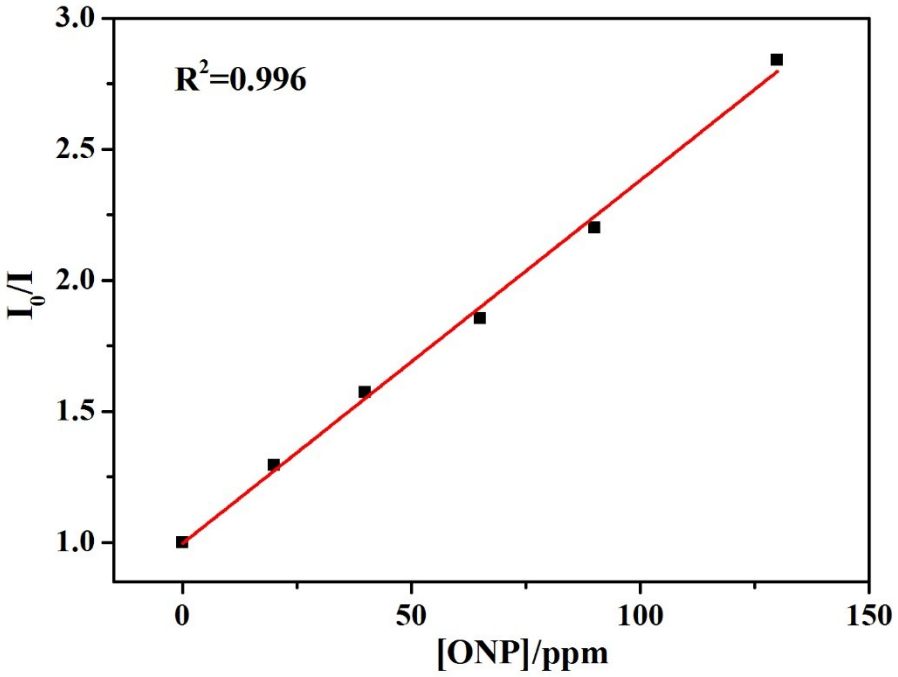

Fig. S32 The Stern–Volmer plot of **1** against MNP.

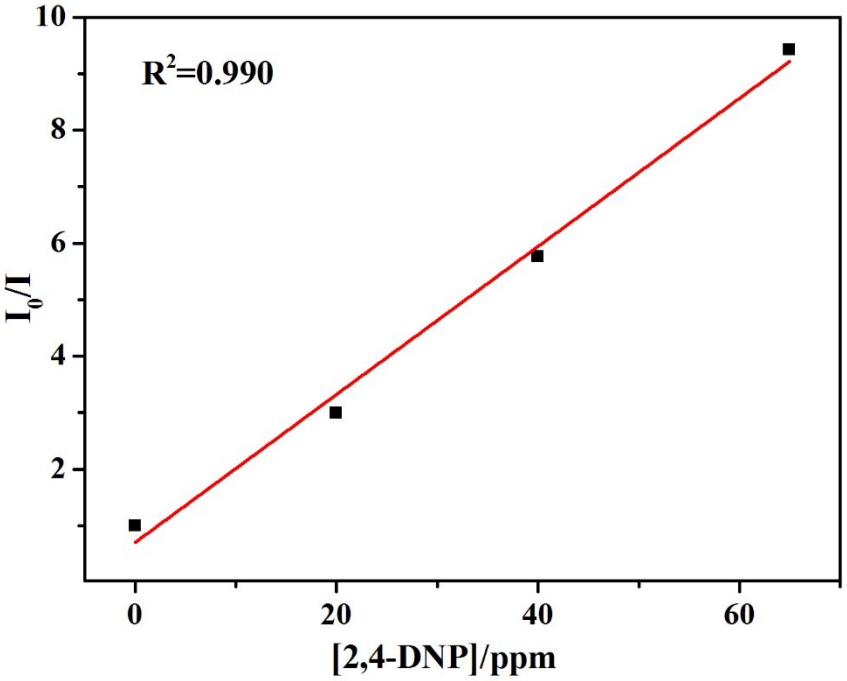

Fig. S33 The Stern–Volmer plot of **1** against 2,4-DNP.

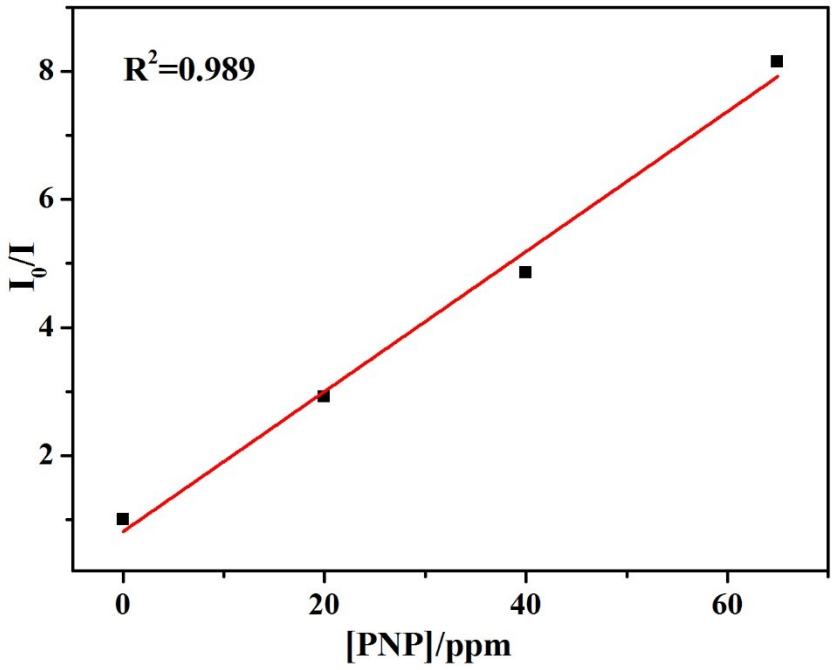

Fig. S34 The Stern–Volmer plot of **1** against PNP.

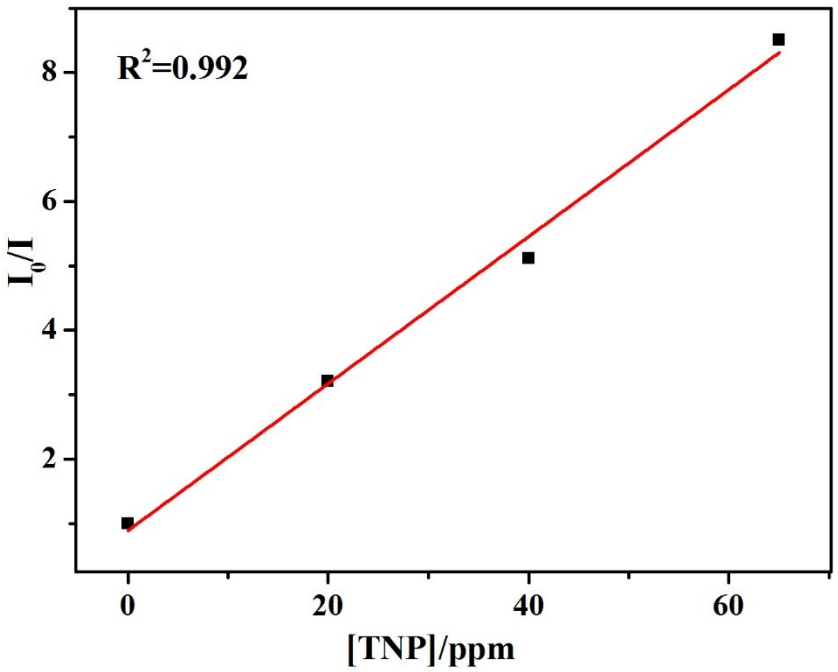

Fig. S35 The Stern–Volmer plot of **1** against TNP.

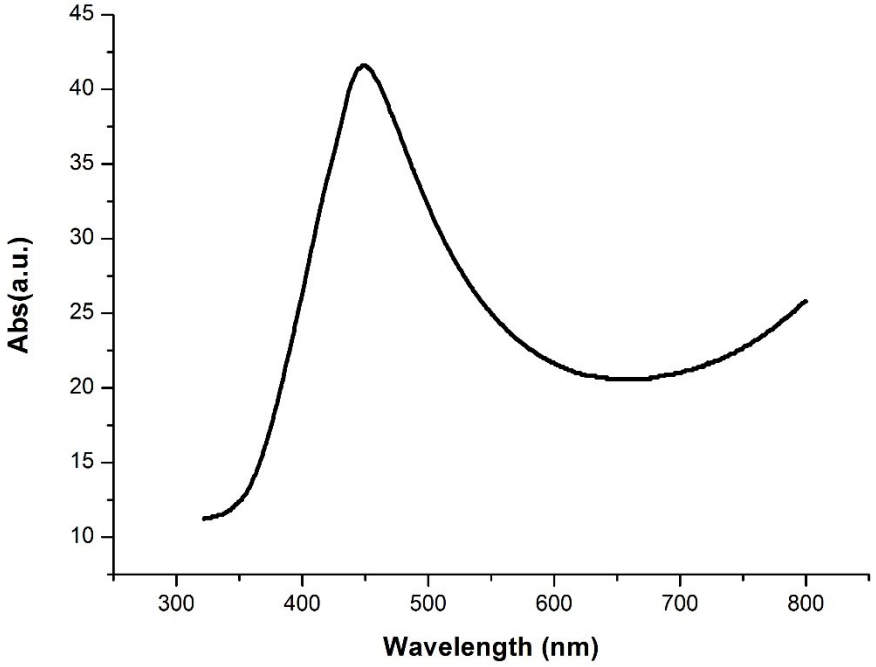

Fig. S36 The UV-vis-NIR spectrum for **1**.

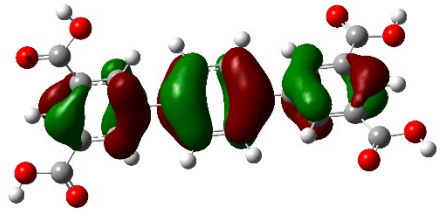 HOMO H_4L	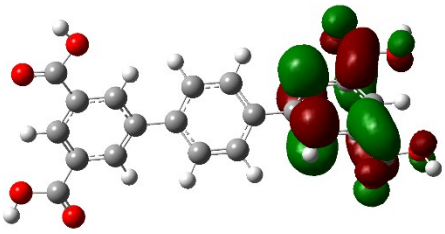 LUMO H_4L
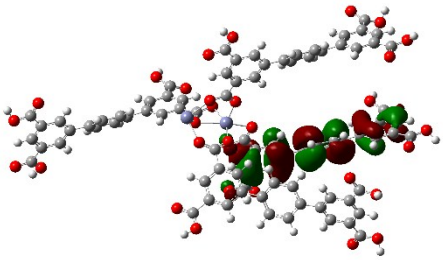 HOMO **1**	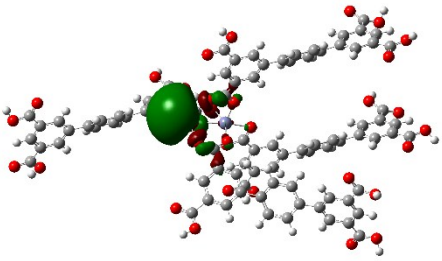 LUMO **1**
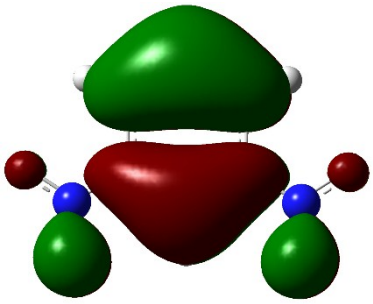 HOMO 1,3-DNB	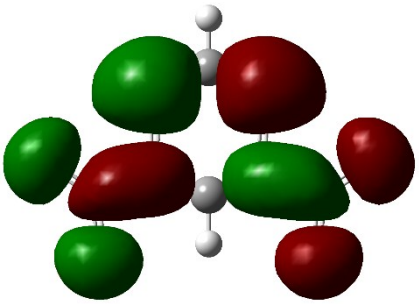 LUMO 1,3-DNB
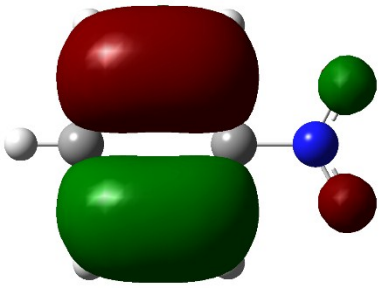 HOMO NB	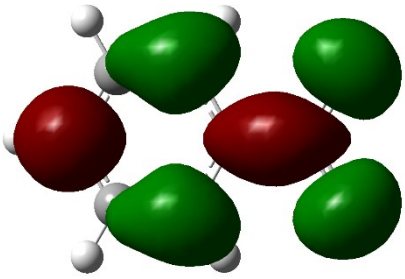 LUMO NB
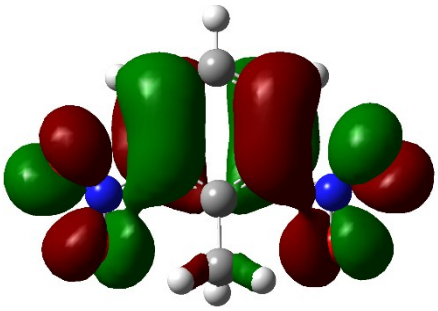 HOMO 2,6-DNT	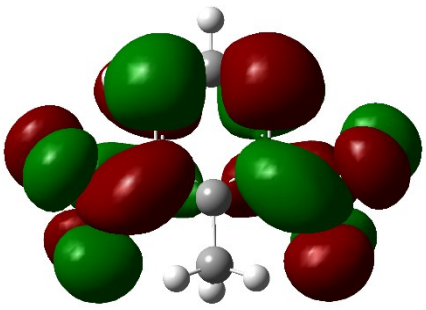 LUMO 2,6-DNT

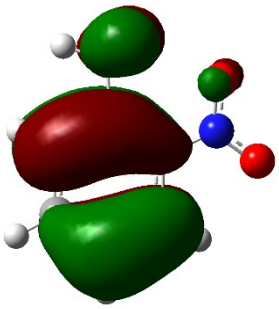 HOMO 2-NT	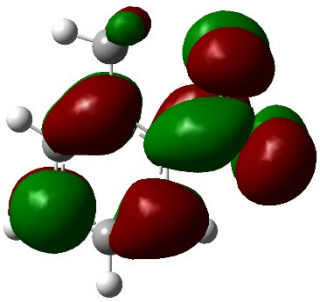 LUMO 2-NT
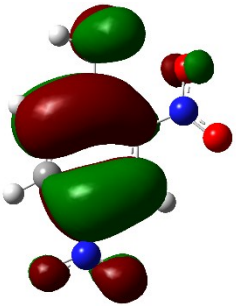 HOMO 2,4-DNT	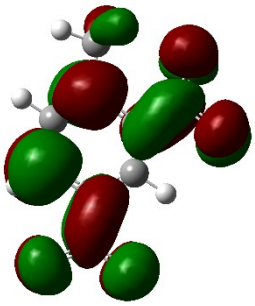 LUMO 2,4-DNT
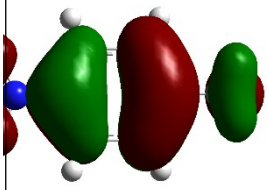 HOMO 4-NT	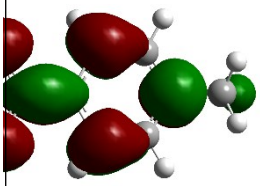 LUMO 4-NT
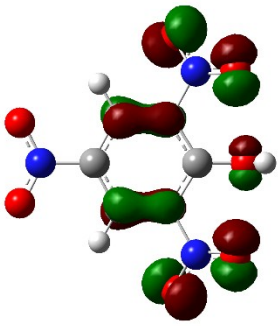 HOMO TNP	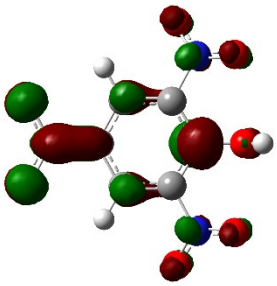 LUMO TNP

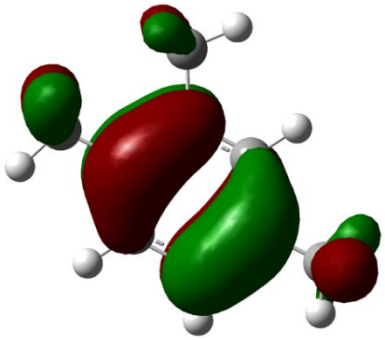 HOMO 1,2,4-TMB	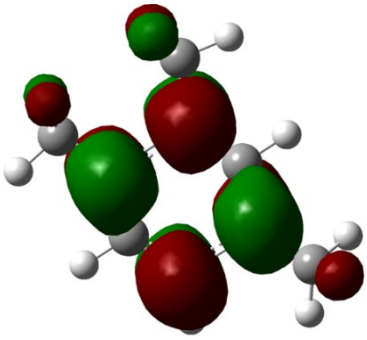 LUMO 1,2,4-TMB
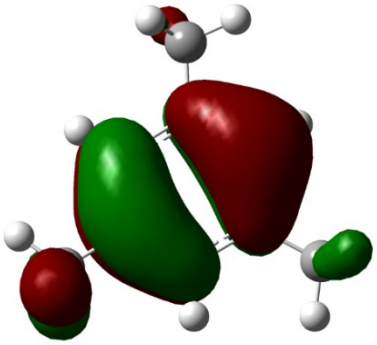 HOMO 1,3,5-TMB	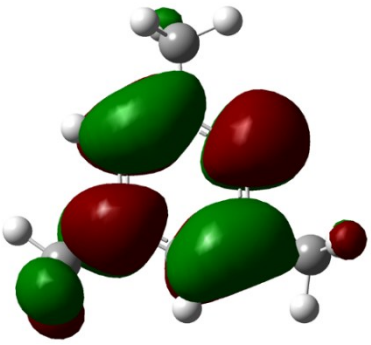 LUMO 1,3,5-TMB
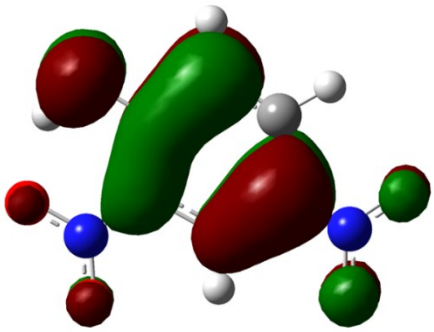 HOMO 2,4-DNP	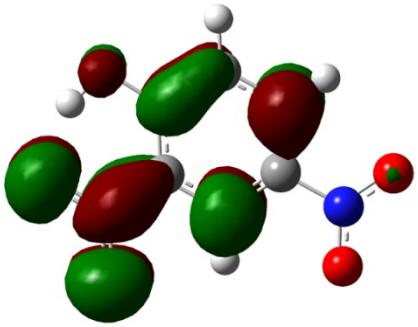 LUMO 2,4-DNP
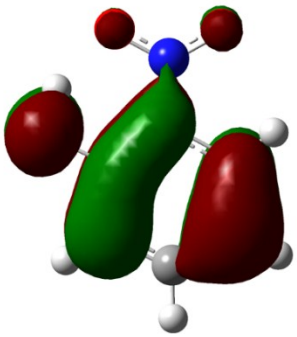 HOMO o-nitro phenol	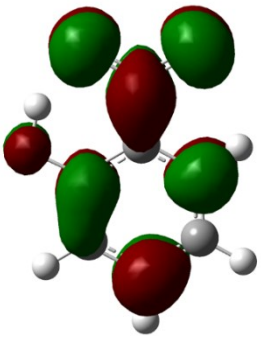 LUMO o-nitro phenol

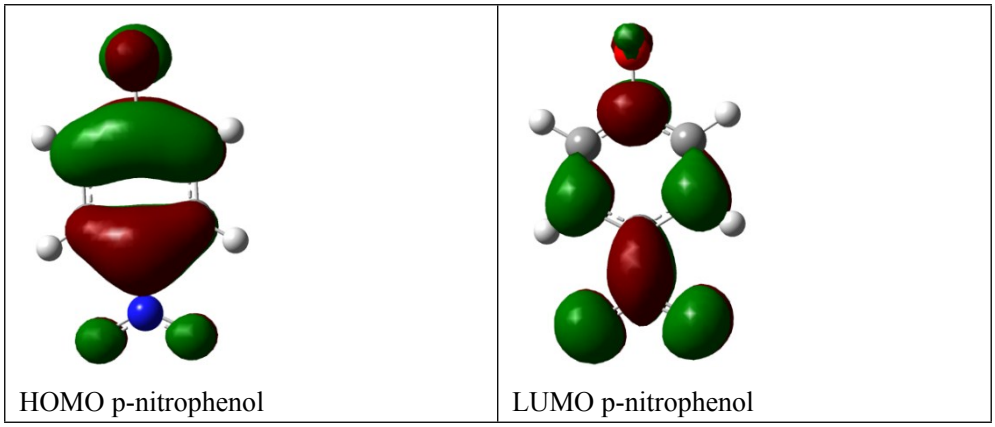

Fig. S37 HOMO-LUMO plots for H_4L, **1** and NACs.

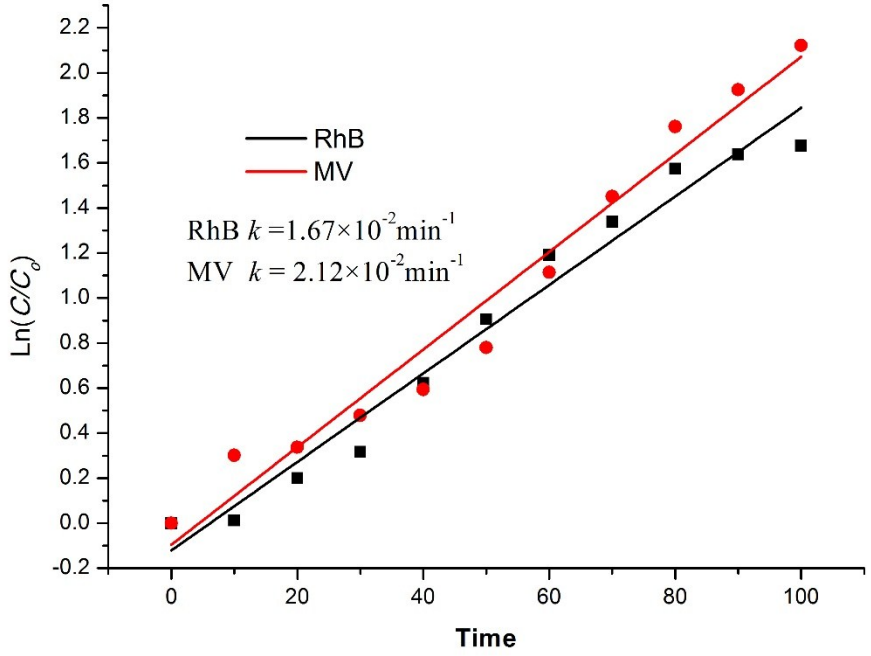

Fig. S38 The plot displaying photocatalytic degradation kinetics of MV/RhB with different concentration of **1**.

Table S1. Crystal data and structure refinement information for **1**

Parameter	**1**
Formula	$C_{23.89}H_{39.07}ZnN_{4.3}O_{10.5}$
Crystal system	monoclinic
Space group	$P\,2_1$
Crystal color	colorless
a, [Å]	9.9954(14)
b, [Å]	16.749(2)
c, [Å]	15.358(2)
α, [°]	90
β, [°]	99.191(3)
γ, [°]	107.444(2)
V, Å ^{3}	90
Z	4
ρ_{calcd}, g/cm^3	1.185
μ, mm^{-1}	1.033
F(000)	906
θ Range, deg	2.86-20.53
Reflection collected	22190/0.0783
Goodness-of-fit on F^2	0.951
R_1, $wR_2(I> 2\sigma(I))^*$	0.0629, 0.1406

R_1, wR_2 (all data)**	0.1166, 0.1680

* $R = \sum(F_o - F_c)/\sum(F_o)$, ** $wR_2 = \{\sum[w(F_o^2 - F_c^2)^2]/\sum(F_o^2)^2\}^{1/2}$.

Table S2. Selected bond distances (Å) and angles (°) of **1**

1

Zn(1)-O(3)	2.034(6)	Zn(1)-O(11)	2.072(7)
Zn(1)-O(7)	2.078(6)	Zn(1)-O(10)	2.111(6)
Zn(1)-O(1)	2.115(6)	Zn(1)-O(9)	2.116(8)
Zn(2)-O(8)	1.960(6)	Zn(2)-O(4)	1.993(7)
Zn(2)-O(5)	2.123(6)	Zn(2)-O(2)	2.137(7)
Zn(2)-O(6)	2.166(7)	Zn(2)-O(1)	2.234(6)
O(3)-Zn(1)-O(11)	175.3(3)	O(3)-Zn(1)-O(7)	96.9(2)
O(7)-Zn(1)-O(11)	171.9(3)	O(1)-Zn(1)-O(11)	90
O(1)-Zn(1)-O(9)	179.9(3)	O(2)-Zn(2)-O(4)	155.1(3)
O(2)-Zn(2)-O(8)	156.0(2)	O(5)-Zn(2)-O(1)	147.4(2)
O(4)-Zn(2)-O(6)	92.5(3)	O(8)-Zn(2)-O(1)	110.1(2)

Table S3 The comparison of the selected materials in detective sensitivity for Fe^{3+} ions

Material	Sensitivity	Reference
$Eu(acac)_3@Zn(C_{15}H_{12}NO_2)_2$	5×10^{-3} M	1
$Eu(C_{33}H_{24}O_{12})(H_2NMe)(H_2O)$	2×10^{-4} M	2
$Eu(C_{22}H_{14}O_2)_3$	10^{-4} M	3
$[Eu(BTPCA)(H_2O)]\cdot2DMF\cdot3H_2O$	10^{-5} M	4
MIL-53(Al)	0.9×10^{-6} M	5
$\{[LnCd_2(DTPA)_2(H_2O)_4]\cdot4H_2O$	1.5×10^{-5} M	6
carbon nanoparticles (CNPs)	0.32×10^{-6} M	7
Fluorescent Gold Nanoclusters	5.4×10^{-6} M	8
$[Cd_3(dpa)(DMF)_2(H_2O)_3]\cdot DMF$	1.75×10^{-4} M	9
$Zn_3L_3(DMF)_2$	10^{-5} M	10
$[[Eu_2(MFDA)_2(HCOO)_2(H_2O)_6]\cdot H_2O$	1.0×10^{-4} M	11
$[Tb_4(OH)_4(DSOA)_2(H_2O)_8]\cdot(H_2O)_8$	10^{-6} M	12
1	2.2×10^{-5} M	*In this work*

References:

[1] G. G. Hou, Y. Liu, Q. K. Liu, J. P. Ma and Y. B. Dong, *Chem. Commun.*2011, ***47***, 10731-10733.

[2] S. Dang, E. Ma, Z.M. Sun and H. J. Zhang, *J. Mater. Chem.* 2012, ***22***, 16920-16926.

[3] M. Zheng, H. Q. Tan, Z. G. Xie, L. G. Zhang, X. B. Jing and Z. C. Sun, *ACS Appl. Mater. Interfaces,* 2013, ***5***, 1078-1083.

[4] Q. Tang, S. X. Liu, Y. W. Liu, J. Miao, S. J. Li, L. Zhang, Z. Shi and Z. P. Zheng, *Inorg. Chem.*2013, ***52***, 2799-2801.

[5] C. X. Yang, H. B. Ren and X. P. Yan, *Anal. Chem.*2013, ***85***, 7441-7446.

[6] Q. Liu, F. Wan, L. X. Qiu, Y. Q. Sun and Y. P. Chen, *RSC Adv.*, 2014, ***4***, 27013-27021.

[7] K. G. Qu, J. S. Wang, J. S. Ren and X. G. Qu, *Chem. Eur. J.* 2013, ***19***, 7243-7249.
[8] J.-A. A. Ho, H.-C. Chang and W.-T. Su, *Anal. Chem*. 2012, ***84***, 3246-3253.
[9] J. C. Jin, L. Y. Pang, G. P. Yang, L. Hou and Y. Y. Wang, *Dalton Trans*., 2015, ***44***, 17222–17228.
[10] Z. C. Yu, F. Q. Wang, X. Y. Lin, C. M. Wang, Y. Y. Fu, X. J. Wang, Y. N. Zhao and G. D. Li, *J. Solid. State. Chem*., 2015, ***232***, 96-101.
[11] X. H. Zhou, L. Li, H. H. Li, T. Yang and W. Huang, *Dalton Trans*., 2013, **42**, 12403–12409.
[12] X. Y. Dong, R. Wang, J. Z. Wang, S. Q. Zang and T. C. W. Mak, *J. Mater. Chem*. A, 2015, ***3***, 641–647.